Journal of Colloid and Interface Science 333 (2009) 242–248

Contents lists available at ScienceDirect

Journal of Colloid and Interface Science

www.elsevier.com/locate/jcis

Electrospinning preparation, characterization and photocatalytic properties of Bi_2O_3 nanofibers

Changhua Wang [a,b], Changlu Shao [c], Lianjia Wang [c], Lina Zhang [c], Xinghua Li [c], Yichun Liu [c,*]

[a] Key Laboratory of Excited State Processes, Changchun Institute of Optics, Fine Mechanics and Physics, Chinese Academy of Sciences, Changchun 130033, People's Republic of China
[b] Graduate University of Chinese Academy of Science, Beijing 100049, People's Republic of China
[c] Centre for Advanced Optoelectronic Functional Materials Research, Northeast Normal University, Changchun 130024, People's Republic of China

ARTICLE INFO

Article history:
Received 29 May 2008
Accepted 26 December 2008
Available online 10 January 2009

Keywords:
Bi_2O_3
Nanofibers
Electrospinning
Photocatalytic

ABSTRACT

Bi_2O_3 nanofibers with diameter of 70–200 nm were successfully prepared by electrospinning a precursor mixture of polyacrylonitrile (PAN)/bismuth nitrate, followed by calcination treatment of the electrospun polymer/inorganic composite fibers. The resulting Bi_2O_3 nanofibers were characterized with X-ray diffraction, X-ray photoelectron spectroscopy, scanning electron microscopy, FT-IR spectra and UV–vis diffuse reflectance spectroscopy. The Bi_2O_3 nanofibers calcined at 500 °C exhibited β phase, and whereas the nanofibers calcined at 550 and 600 °C both exhibited dominant β phase together with a trace amount of α phase. Photocatalytic experiments indicated that the obtained Bi_2O_3 nanofibers calcined at 500 °C were highly active for photodegradation of organic pollutants Rhodamine B (RB). Furthermore, the Bi_2O_3 nanofibers could be easily recycled without decrease of the photocatalytic activity.

1. Introduction

Low dimensional metal oxide nano-structured materials continue to draw increasing attention and find uses in an increasing number of potential applications in many fields such as catalysis, electronics and photonics [1–3]. Therein, owing to the urgent need for a clean and comfortable environment, various nano-structured semiconductor materials, especially, have been exploited and used as heterogeneous photocatalysts for various environmental-related applications including the remediation of environmental pollutants through photocatalytic reaction [4–8]. Among various oxide semiconductor photocatalysts, recently, nano-structural Bi_2O_3 has been proven to be a valuable photocatalyst, that is, Bi_2O_3 nanoparticles or thin films can be effective, efficiently breaking down RB and methyl orange pollutant in water under UV and visible light, respectively [9–11]. However, the use of bismuth oxide nanoparticles with high surface area for photocatalysis is often limited, because the suspended particulate catalysts are easily lost in the process of photocatalytic reaction and separation, which may re-pollute treated water again. In addition, though Bi_2O_3 films can be fixed and reclaimed easily, but have been fabricated through tedious and costly process. Instead of the corresponding nanoparticles and thin films, nanofibers being an important subclass of *nanostructural* materials are deemed as potential good candidates for practical application due to their high photocatalytic activity and favorable recycling characteristics [12].

Recently, TiO_2 nanofibers do open a wide range of new possibilities of high photocatalytic activity and easy recovery [13,14]. Nevertheless, to the best of our knowledge, little work has been reported on the Bi_2O_3 nanofibers up until now. In view of this, we prepared Bi_2O_3 nanofibers via a novel and simple approach called electrospinning technique. The electrospinning technique is a versatile and effective method for the preparation of polymer fibers, inorganic and hybrid compounds nanofibers. Among these methods, fabricating inorganic fibers intrigues many scientists during the past several years [15–18]. A typical electrospinning procedure consists of three major steps: (1) preparation of an inorganic sol or a solution containing a polymer together with an alkoxide or salt; (2) electrospinning of the solution to prepare nanofibers of polymer/inorganic composites; (3) calcinations of the composite fibers to obtain the desired inorganic nanofibers. In this work, Bi_2O_3 nanofibers are prepared by electrospinning a precursor mixture of PAN/$Bi(NO_3)_3$, followed by careful sintering of the electrospun polymer/inorganic composite fibers at different temperature for 10 h. Such a method can also be extended to preparation of BiOCl nanofibers photocatalysts by simply replacing PAN/$Bi(NO_3)_3$ precursor with PAN/$BiCl_3$ precursor. The as-prepared nanofibers exhibit catalytic properties, and as long fibers can be reclaimed easily, so they may serve as good potential candidates for photocatalytic application.

* Corresponding author. Fax: +86 431 5684009.
E-mail address: ycliu@nenu.edu.cn (Y. Liu).

0021-9797/$ – see front matter
doi:10.1016/j.jcis.2008.12.077

2. Materials and methods

2.1. Materials preparation and characterization

A PAN solution of 10 wt% was first prepared by dissolving PAN powder in *N*,*N*-dimethyl formamide and stirring for 2 h. In the preparation of a PAN/$Bi(NO_3)_3$ solution, 1 g of $Bi(NO_3)_3$ was dissolved in 20 mL of as-prepared PAN solution, followed by vigorously stirring at room temperature for 4 h to form a homogeneous viscous solution. The viscous solution thus obtained was drawn into a plastic syringe equipped with a capillary. A copper pin connected to a high-voltage generator was placed in the solution. The solution was fed at a rate of 1.0 mL/h using a motor syringe pump. A piece of flat aluminum foil was placed about 10 cm below the tip of the needle to collect the nanofibers. Non-woven mat structure of composite PAN/$Bi(NO_3)_3$ nanofibers was fabricated by applied electric voltage of 10 kV between the collector and the needle tip. The electrospinning was conducted in air at room temperature. Finally, the electrospinning nanofibers were calcined in air at 500, 550, 600 °C, respectively, at a heating rate of 2 °C/min and remained at the required temperature for 10 h to obtain Bi_2O_3 nanofibers.

FT-IR spectra were obtained on Magna 560 FT-IR spectrometer with a KBr disk. Thermal analysis was carried out to study thermal stability of the samples using NETZSCH STA 449C thermoanalyzer in air in the temperature range of 0–600 °C at a heating rate of 10 °C/min. UV–vis/DR spectra of the samples were recorded on a Cary 500 UV–VIS–NIR spectrophotometer and $BaSO_4$ was used as a reference. Samples were crushed manually and yielded into fine powders using an agate mortar. XRD patterns of the samples were recorded on a Rigaku, D/max-2500 X-ray diffractometer operated at 40 kV and 100 mA using Cu$K\alpha$ radiation. X-ray photoelectron spectroscopy (XPS) was performed on a VG-ADES 400 instrument with Mg$K\alpha$-ADES ($h\nu = 1253.6$ eV) source at a residual gas pressure of below 10^{-8} Pa. Quantifications of the elements were performed with relative sensitivity factor method, adopting following factors: 7.4 for Bi4f, 0.66 for O1s and 0.25 for C1s. The field emission SEM (FESEM) was performed on a Hitachi S-4800 FESEM field emission scanning electron microscope.

2.2. Photocatalytic test

The photoreactor was designed with an internal light source (50 W high pressure mercury lamp with main emission wavelength 313 nm) surrounded by a quartz jacket, where the suspension includes the nanofibers catalyst and an aqueous RB (100 mL, 20 mg/L) completely surrounded the light source. The suspension was stirred in the dark for 30 min to obtain a good dispersion and establish adsorption–desorption equilibrium between the organic molecules and the catalyst surface. The acidity of the suspension was neutral. The temperature of the suspension was maintained at 30 ± 2 °C by circulation water through an external cooling coil, and the system was open to air. Decreases in the concentrations of dyes were analyzed by a Cary 500 UV–VIS–NIR spectrophotometer at $\lambda = 553$ nm. At given intervals of illumination, the samples of the reaction solution were taken out, and then centrifuged and filtrated. Finally, the filtrates were analyzed.

3. Results and discussion

3.1. Physicochemical characterization

Fig. 1 shows the XRD patterns of the as-prepared Bi_2O_3 nanofibers calcined at different temperature. It is known that bismuth oxides have polymorphism: six modifications, which are α, β, γ, δ, ε and ω-Bi_2O_3. Among them, α phase is stable at low temperature, δ phase is stable at high temperature and the other

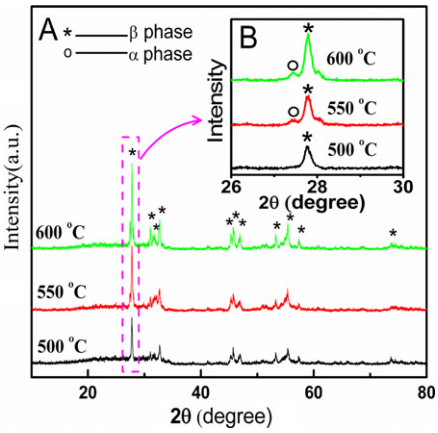

Fig. 1. (A) XRD patterns of Bi_2O_3 nanofibers annealed at different temperatures. (B) Enlargement of the region around 27.5° 2θ of different fibers.

phases are high temperature metastable. In our case, all the Bi_2O_3 nanofibers mainly exhibit metastable β phase (JCPDS 76-147) as can be seen from the spectra (Fig. 1A) with characteristic 2θ values at 27.66° (201), 29.96° (211), 31.11° (002), 32.75° (220), 45.88° (222), 47.03° (400), 53.42° (203), 55.39° (421), 57.36° (402), 73.77° (423), 74.76° (224), 75.74° (601), respectively. Furthermore, a trace amount of α-Bi_2O_3 (JCPDS 76-1730) with characteristic 2θ values at 27.45° (120) is detected in the samples calcined at 550 and 600 °C, respectively (Fig. 1B). In addition, XRD analysis shows that both β and α phase become perfect with the increase of calcination temperature. It has been reported that the phase composition of Bi_2O_3 is strongly influenced by the synthesis route and phase transition usually happens. Monnereau et al. [19] obtained β-Bi_2O_3 by decomposition of Bi(III)-oxalate between 250 and 300 °C, thus obtained β-Bi_2O_3 was stable up to ~300 °C at which temperature transition to α-Bi_2O_3 was observed. Gotić et al. [20] prepared β-Bi_2O_3 by modified sol–gel procedure, upon increase in heating temperature to 500 °C, α-Bi_2O_3 was detected. They pointed out that higher times of heating the precursor at 400 °C or 500 °C in O_2 atmosphere induced a phase transition β-$Bi_2O_3 \rightarrow \alpha$-$Bi_2O_3$. Bedoya et al. [21] reported the deposition processes of bismuth oxides using $Bi(C_6H_5)_3$ precursor, the Bi_2O_3 films deposited over Pt substrate mainly exhibited either tetragonal phase or cubic phase at 400 °C, and whereas at 500 °C, films consisted mainly of the monoclinic phase with a few traces of the cubic phase. They explained that crystalline phase mainly depended on the deposition temperature. Therefore, in the present work, the phase transition is thought to be mainly caused by the changes in temperature dependence. That is, phase transition β-$Bi_2O_3 \rightarrow \alpha$-$Bi_2O_3$ occurred when the Bi_2O_3 nanofibers were calcined above 500 °C for 10 h. The proportion of β-Bi_2O_3 phase in as-prepared Bi_2O_3 nanofibers can also be roughly estimated from the ratio of intensity of (201) peak (β phase) to the sum of those of (201) peak (β phase) and (120) peak (α phase). It is calculated that the proportion of β phase is 85.6% and 76.7% for Bi_2O_3 nanofibers calcined at 550 and 600 °C, respectively.

In Fig. 2 is shown the thermal behavior of different nanofibers. As observed in Fig. 2A, pure PAN nanofibers show poor heat resistance with no residue above 460 °C. By comparing the TG curves of the as-spun PAN and PAN/$Bi(NO_3)_3$ composite nanofibers, it can be deduced that the four obvious weight losses appearing at 25–282, 282–317, 317–406, 406–460 °C in the TG curve of PAN/$Bi(NO_3)_3$ composite nanofibers are ascribed to the evaporation of the absorbed water and the thermal decomposition of the organics. Above 460 °C, there is no further weight loss, confirming the completely decomposition of the organics.

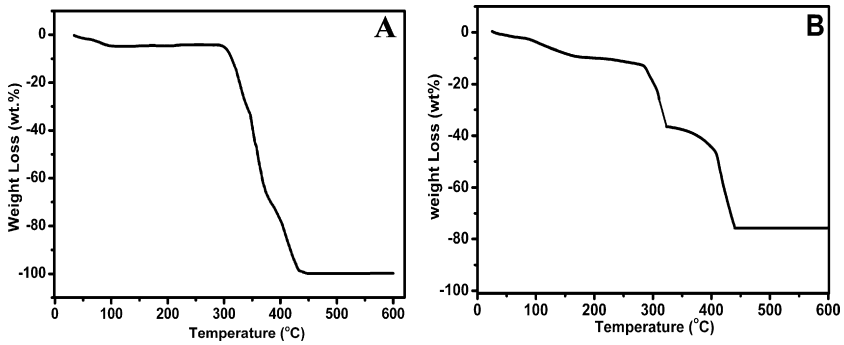

Fig. 2. TG curve of thermal decomposition of (A) PAN nanofibers. (B) PAN/$Bi(NO_3)_3$ composite nanofibers at a heating rate of 10 °C/min in the air.

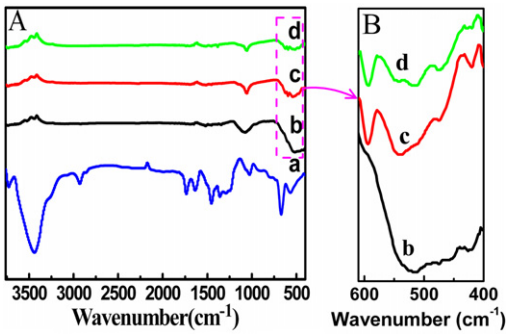

Fig. 3. (A) FT-IR spectra of various samples: (a) the as-spun PAN/$Bi(NO_3)_3$ composite fibers, (b) Bi_2O_3 nanofibers calcined at 500 °C, (c) Bi_2O_3 nanofibers calcined at 550 °C, (d) Bi_2O_3 nanofibers calcined at 600 °C. (B) IR characteristic peaks of different Bi_2O_3 nanofibers lie in the region of 400–600 cm^{-1}.

The obtained Bi_2O_3 nanofibers were characterized by FTIR spectra to prove the removal of the polymer and the results are shown in Fig. 3A. Fig. 3Aa shows the IR spectrum of PAN/$Bi(NO_3)_3$ nanofibers. The bands in the regions 2931–2870, 1460–1450, 1380–1350, and 1270–1220 cm^{-1} are assigned to the aliphatic CH group vibrations of different modes in CH, CH_2, and CH_3. Fig. 3A, spectra b–d, shows the spectra of Bi_2O_3 nanofibers calcined at different temperature for 10 h, it is found that the characteristic peaks of the PAN has been disappeared (compared with Fig. 3Aa), indicating that the organic molecules could be removed completely from PAN/bismuth nitrate composite fibers. Additionally, several new peaks from 400 to 600 cm^{-1} attributed to vibration of Bi–O bonds of BiO_6 octahedra [22] display in the spectra of different Bi_2O_3 nanofibers, indeed confirming the formation of Bi_2O_3 nanofibers. Fig. 3B shows the enlarged IR spectra of different nanofibers in the region of 400–600 cm^{-1}. It can be obviously observed that an additional peak at 595 cm^{-1} (Fig. 3B, spectra c–d) appears in the Bi_2O_3 nanofibers annealed at 550 and 600 °C compared with that annealed at 500 °C (Fig. 3Bb). The additional peak at 595 cm^{-1} is reported to be the vibration of Bi–O bonds of BiO_6 coordination polyhedra in α-Bi_2O_3 [23], which is well consistent with the results of XRD above. Besides, it needs to mention that an absorption band at about 1060 cm^{-1} is also observed in Fig. 3A, spectra b–d. As organic molecules are removed completely, this absorption band may be attributed to the other kinds of vibrations of Bi–O caused by the interaction between the Bi–O bonds and their other surroundings. Moreover, the width of the peak at 1060 cm^{-1} show somewhat decrease with the increase of calcinations temperature. That is, the Bi_2O_3 nanofibers calcined at 500 °C show a broader IR characteristic peak than that calcined at 550 and 600 °C. This may result from the smaller size of Bi_2O_3 nanoparticles calcined at 500 °C compared with that calcined at 550 and 600 °C [24].

XPS survey scan of the as-prepared fibers (Fig. 4A) revealed the presence of Bi, O and C in the as-prepared Bi_2O_3 nanofibers.

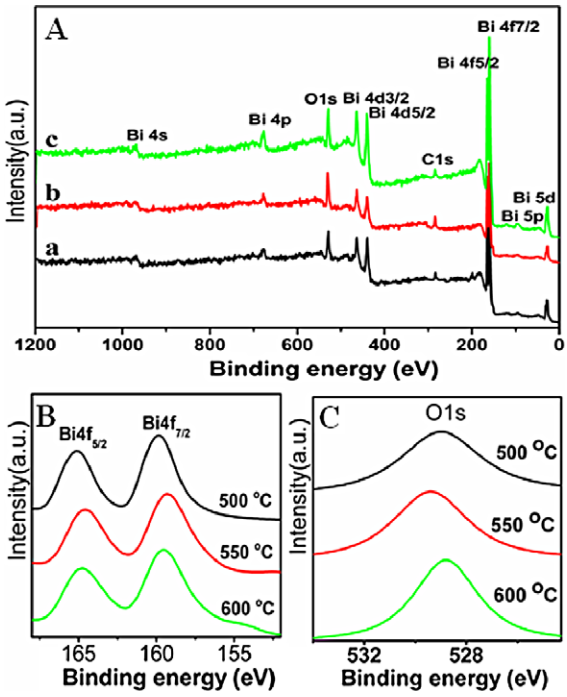

Fig. 4. (A) XPS survey spectra for the surface of Bi_2O_3 nanofibers calcined at different temperature. (B) High-resolution XPS spectra of Bi4f in different Bi_2O_3 nanofibers. (C) High-resolution XPS spectra of O1s in different Bi_2O_3 nanofibers.

Since the polymer PAN has been degraded completely at 500 °C, as confirmed by TG and IR analysis above, the C1s peak located at 284.8 eV in the XPS spectra is derived from a surface layer of contamination carbon. Moreover, the C1s peak at 286.5 eV and N1s peak at 399.8 eV for the species associated with –C≡N groups of PAN [25] are not detected, confirming that the organic species are removed completely once again. The elements analysis results are summarized in Table 1. The quantification of the XPS peaks for the three samples gives the Bi/O atomic ratio of about 1.0:1.5, which is nearly consistent with the given formula of Bi_2O_3. The high resolution spectra of Bi4f and O1s in Bi_2O_3 nanofibers annealed at different temperatures are displayed in Figs. 4B and 4C, respectively. On the one hand, it can be seen that the XPS peaks of Bi4f shift to lower binding energy as the calcination temperature increase from 500 to 550 °C. The observed shift may be due to the inclusion of α phase Bi_2O_3 in the β-Bi_2O_3 nanofibers, which is accordance with the results of XRD and IR. This is also in agreement with the results obtained by Wu et al. [9]. They pointed out that the thin tetragonal phase bismuth oxide films had bigger binding energy than that of monoclinic phase films. On the contrary, the binding energy of Bi4f for Bi_2O_3 nanofibers calcined at 600 °C slightly shifts to a higher value compared with Bi_2O_3 nanofibers

Table 1
Binding energy (eV) of Bi4f, O1s, C1s peaks and elements analysis results of different Bi_2O_3 nanofibers. n(Bi):n(O):n(C) denotes the atomic number ratio of element Bi to O to C. w (%) denotes the weight percentage of each element.

Sample	Binding energy (eV)				n(Bi):n(O):n(C)	w(Bi) (%)	w(O) (%)	w(C) (%)
	$Bi4f_{7/2}$	$Bi4f_{5/2}$	O1s	C1s				
Bi_2O_3-500 °C	159.9	165.2	529.0	284.8	1:1.48:0.85	86.05	9.75	4.20
Bi_2O_3-550 °C	159.3	164.6	529.4	284.8	1:1.52:1.19	84.41	9.82	5.77
Bi_2O_3-600 °C	159.6	164.9	528.7	284.8	1:1.54:0.97	85.21	10.05	4.74

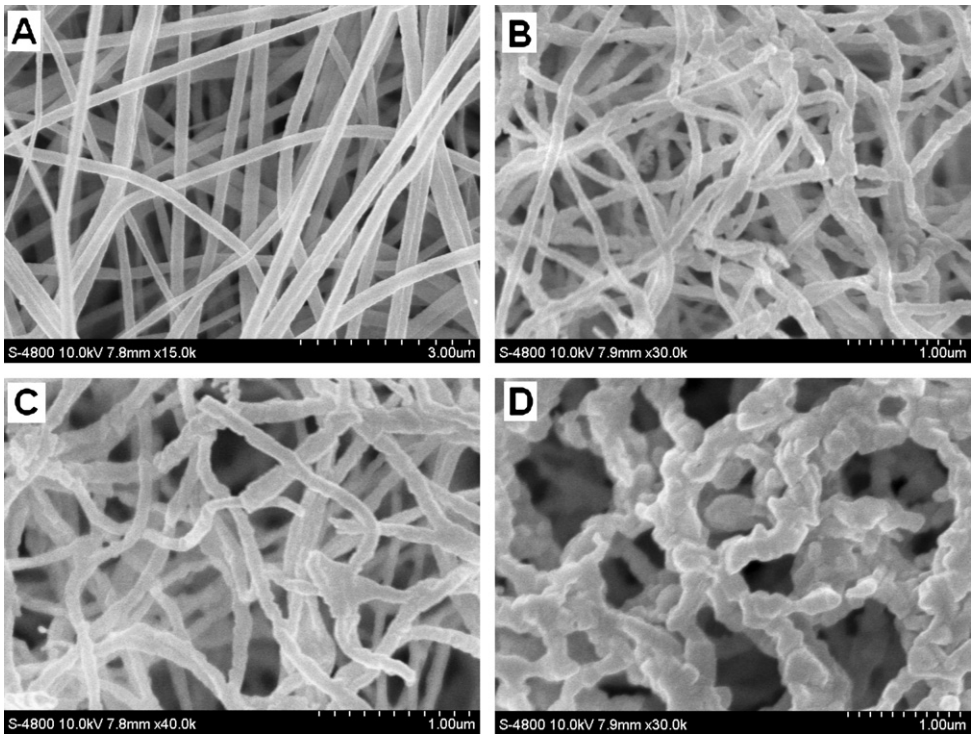

Fig. 5. SEM images of (A) as-spun PAN/$Bi(NO_3)_3$ composite fiber, (B) Bi_2O_3 nanofibers calcined at 500 °C, (C) Bi_2O_3 nanofibers calcined at 550 °C, (D) Bi_2O_3 nanofibers calcined at 600 °C.

calcined at 550 °C, while that of O1s shifts to a lower value, which is mainly due to the increase in the crystallinity of Bi_2O_3 with the increase of calcination temperature [26], as mentioned in XRD analysis.

Morphologies of as-prepared nanofibers were characterized by FESEM (Fig. 5). Fig. 5A shows the SEM micrograph of the electrospun composite fibers. It can be observed that these randomly oriented fibers have smooth and uniform surface due to the amorphous nature of the PAN/$Bi(NO_3)_3$ composite nanofibers. Their lengths can reach several micrometers and diameters range from 200 to 300 nm. The Bi_2O_3 nanofibers exhibit shrinkage resulting from the decomposition of PAN and the removal of the nitrate content of $Bi(NO_3)_3$. For this, the diameters of Bi_2O_3 nanofibers calcined at 500 °C (Fig. 5B) range from 70 to 100 nm, the diameters of Bi_2O_3 nanofibers calcined at 550 °C (Fig. 5C) range from 120 to 150 nm, and the diameters of Bi_2O_3 nanofibers calcined at 600 °C (Fig. 5D) range from 150 to 200 nm, respectively. It is also found that the diameters of Bi_2O_3 nanofibers increase with the increase of calcinations temperature, which can be explained by the fact that the grains of Bi_2O_3 gradually grow larger as the sintering temperature becomes higher. Interestingly, a change in fiber morphology is observed after increasing temperature to 600 °C. By carefully watching the surface of these nanofibers, it can be found that the nanofibers appear to consist of linked particles or crystallites, which is related to a dramatic change in crystal structure as observed in other electrospun nanofibers such as V_2O_5 [27] and $NaCo_2O_4$ [28], etc.

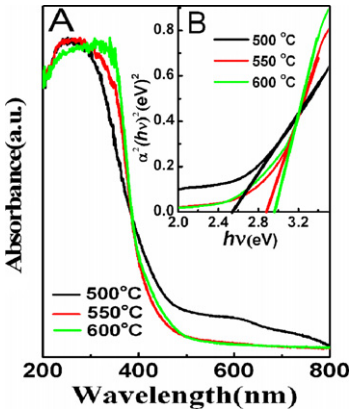

Fig. 6. (A) UV–vis/DR of different Bi_2O_3 nanofibers. (B) Plots of $(\alpha h\nu)^2$ versus energy ($h\nu$) for the band gap energies.

The different phase composition also had significant effect on the optical absorption property of Bi_2O_3, which was confirmed by UV–vis/DR. According to the spectra (Fig. 6A), all the as-prepared nanofibers present the photoabsorption properties from UV light region to visible light shorter than 470 nm, which is assigned to the intrinsic band gap absorption. The small absorption peak at around 600 nm for the Bi_2O_3 nanofibers calcined at 500 °C is probably caused by impurity or defects levels and the amorphous nature of the sample. Furthermore, shifts in the absorption edge

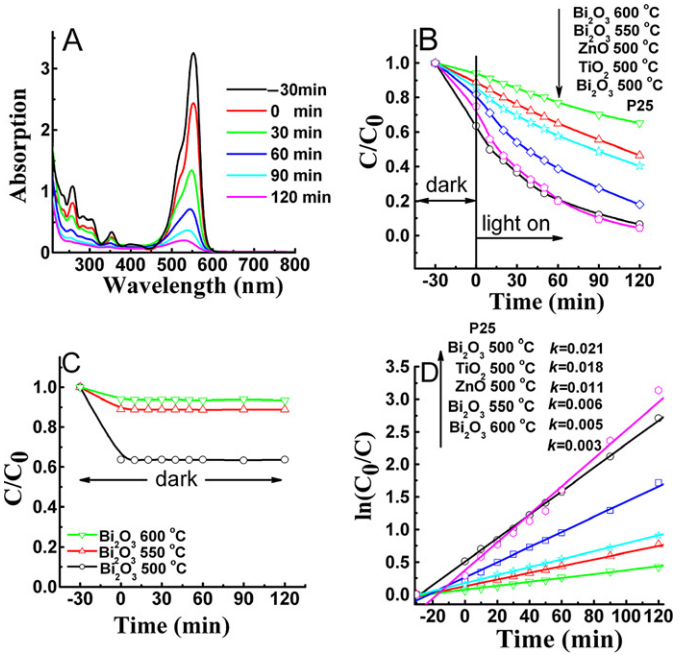

Fig. 7. (A) Adsorption spectra of RB solutions in the presence of Bi_2O_3 nanofibers calcined at 500 °C under UV-light at different periods of time. (B) Degradation profiles of RB over different fibers and P25. $C_0 = 20$ mg/L, catalyst 0.08 g. (C) Curve of changes of concentration of RB solutions in the presence of Bi_2O_3 nanofibers calcined at 500, 550 and 600 °C without UV light irradiation at different periods of time. (D) Kinetic linear simulation curves of RB photocatalytic degradation with different fibers and P25.

among the three samples are observed. The band gap energy of the as-prepared fibers is determined from a plot of $(\alpha h\nu)^2$ versus energy $(h\nu)$ and is found to be about 2.55, 2.88 and 2.97 eV for Bi_2O_3 nanofibers calcined at 500, 550 and 600 °C, respectively (Fig. 6B). In other word, the higher calcination temperature is, the wider absorption band of Bi_2O_3 nanofibers show, the larger band gap energy of Bi_2O_3 nanofibers have. Since the band gap of α-Bi_2O_3 is equal to 2.85 eV, while that of β-Bi_2O_3 is 2.58 eV, and the energy gap may change from about 2 to 3.96 eV, depending on the preparation technology [29], herein, it is believed that the inclusion of α-Bi_2O_3 in the Bi_2O_3 nanofibers with the predominant phase being β-Bi_2O_3 contribute to the observed blue shift of the band gap from 2.55 to 2.97 eV.

3.2. Photocatalytic activity

The photocatalytic activities of Bi_2O_3 nanofibers were evaluated by photo-oxidation of aqueous Rhodamine B (RB). Two control experiments were performed under the conditions: (1) with UV-light irradiation but in the absence of photocatalysts; and (2) in the presence of Bi_2O_3 nanofibers but in the dark. The results obtained here have demonstrated that the Bi_2O_3 nanofibers are active and efficient photocatalysts for the degradation of RB. As shown in Fig. 7A, the major absorption band of RB shifts from 553 to 527 nm step by step under UV-light in the presence of Bi_2O_3 nanofibers calcined at 500 °C, indicating removal of ethyl groups one by one, which is in good accordance with that in the literature [30]. At the same time, the color of the suspension changes gradually, demonstrating that the chromophoric structure of the dye is destroyed. The plot for the concentration changes of RB is shown in Fig. 7B. 93, 54 and 35% degradation of RB is observed after 120 min irradiation for Bi_2O_3 nanofibers calcined at 500, 550 and 600 °C respectively. Among the three nanofibers, Bi_2O_3 nanofibers calcined at 500 °C are the most active, and the photocatalytic activity decreases with the increase of annealed temperature from 500 to 600 °C. The curve plotted in the presence of Bi_2O_3 nanofibers calcined at 500, 550 and 600 °C but in the dark (Fig. 7C) shows only 36%, 11% and 7% decolorization after 120 min, respectively, confirming that the decolorization of RB solutions was not dominated by surface adsorption but by photodegradation.

Concerning the potential applicability of the Bi_2O_3 nanofibers as photocatalysts, a series of further comparative experiments were carried out. It is well known that anatase TiO_2 and hexagonal ZnO possess good photocatalytic activities. So TiO_2 and ZnO nanofibers [12,31] were prepared by electrospinning method for comparison. Commercial TiO_2 powders (P25; from Degussa) was also tested as a reference. SEM results reveal that the diameters of TiO_2 nanofibers range from 170 to 210 nm (Fig. S1A) and the diameters of ZnO nanofibers range from 200 to 300 nm (Fig. S1B). XRD patterns indicate that TiO_2 nanofibers exhibit anatase phase (JCPDS 71-1167, Fig. S2A), and ZnO nanofibers exhibit hexagonal phase (JCPDS 89-511, Fig. S2B). The curves of photocatalytic degradation of RB over these two kinds of nanofibers are shown in Fig. 7B. It can be noticed that the performance of Bi_2O_3 nanofibers calcined at 500 °C is much better than those of both TiO_2 and ZnO nanofibers calcined at 500 °C. More importantly, the photoactivity of Bi_2O_3 nanofibers calcined at 500 °C is close to that of commercial P25 powders. Therefore, it can be safely concluded that the good performance of Bi_2O_3 nanofibers in photodegrading organic dye RB is significant for the environmental remediation and photocatalysis applications.

The decomposition kinetics is understood according to physical chemistry principles, and the kinetic linear simulation curves of RB photocatalytic degradation over different Bi_2O_3 nanofibers are displayed, together with those of TiO_2, ZnO nanofibers and P25. The results show that the above degradation reactions follow a Langmuir–Hinshelwood apparent first-order kinetics model due to the low initial concentrations of the reactants [32]. The explanation is described below.

$$r = dC/dt = kKC/(1 + KC), \tag{1}$$

where r is the degradation rate of the reactant (mg/(L min)), C the concentration of the reactant (mg/L), t the UV-light illumination time, k the reaction rate constant (mg/(L min)), and K the adsorption coefficient of the reactant (L/mg). When the initial concentration (C_0) is very low ($C_0 = 20$ mg/L for RB in the present experiment), Eq. (1) can be simplified to an apparent first-order model

$$\ln C_0/C = kKt = k_{app}t, \tag{2}$$

where k_{app} is the apparent first-order rate constant (min^{-1}) [33]. The determined k_{app} for different catalysts is shown in Fig. 7D. It is clearly demonstrated that Bi_2O_3 nanofibers calcined at 500 °C have better performance than TiO_2 and ZnO nanofibers calcined at 500 °C, because it's lowering rate in C/C_0 is higher than those of TiO_2 and ZnO nanofibers, which further confirm the results of the activity studies above.

On the basis of the above experimental results and the characteristics of as-prepared Bi_2O_3 nanofibers in morphology, structure, and optical properties, we infer that several factors could contribute to the difference of the photocatalytic efficiency. Firstly, it is known that the process for photocatalysis of Bi_2O_3 is the direct absorption of photon by its band gap and generates electron–hole pairs in the Bi_2O_3 nanoparticles [10], the excitation of an electron from the valence band to the conduction band is initiated by light absorption with energy equal to or greater than the band gap of Bi_2O_3. Upon excitation, the separated electrons and holes can follow surface of solid. Therefore, the narrower band gap, the easier it is to excite electrons from the valence band to the conduction band [34]. The difference in the band gap thus leads to different photocatalytic behavior. In this work, Bi_2O_3 nanofibers

calcined at 500 °C with narrower band gap compared with that of Bi_2O_3 nanofibers calcined at 550 and 600 °C can absorb more light and thus more electrons and holes are generated, then these electrons and holes have redox activities, and the photogenerated holes can react with surface hydroxyl groups to produce the free radicals of $OH^{\bullet}$. The radical of $OH^{\bullet}$ can not only oxidize the adjacent organic compound, but also be diffused into the solution and oxidize the organic compounds. Secondly, the thinner fibers with higher surface area may also play an important role in the enhancement of their photocatalytic activities. Bi_2O_3 nanofibers calcined at 500 °C with thinner fibers which ensure higher exposure to the UV light can provide more active sites and absorb more reactive species than those calcined at 550 and 600 °C. It is also noteworthy that there is another possibility to account for the better performance in the photocatalytic activity of Bi_2O_3 nanofibers calcined at 500 °C. That is, crystallinity and photoactivity are inextricably linked. It has been demonstrated that defects may serve as recombination centres for photoexcited electron–hole pairs during photocatalysis, thereby decreasing the photocatalytic activity [35]. In other word, the better the crystallinity, the fewer defects there are, resulting in good photocatalytic activity. This may explain why Bi_2O_3 nanofibers exhibiting pure β phase possess higher activity. Despite the above identified factors, we still recognize that the very complex nature of the photocatalytic activity remains to be fully explored. Further studies are necessary to clarify the effects of the band gap energy, surface area and crystalline composition of Bi_2O_3 on the photocatalytic activity.

Seeing that the feasibility of separation of catalyst from solution after reaction is of crucial importance, sedimentation ability of the Bi_2O_3 nanofibers as well as P25 powders were tested. In this experiment, the nanofibers catalysts with lengths at scale of micrometers sedimentated from an aqueous suspension after photocatalytic reaction in less than 1 h, while the aqueous suspension of P25 powders was still turbid even after 2 h. Meanwhile, long-term stability of Bi_2O_3 nanofibers was investigated. Fig. 8 shows photocatalytic degradation of RB over the Bi_2O_3 nanofibers calcined at 500 °C with three time cycling uses and indicates no obvious decrease for photoactivity. This fact that the nanofibers photocatalysts with high photocatalytic activity could be easily recovered by sedimentation will greatly promote their industrial application to eliminate the organic pollutants from wastewater.

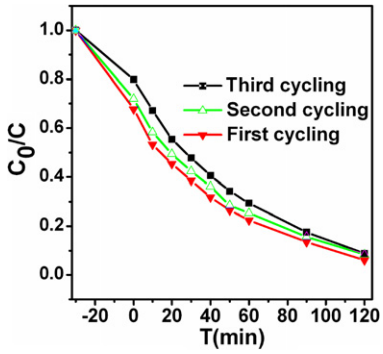

Fig. 8. Photocatalytic activity of the Bi_2O_3 nanofibers calcined at 500 °C for RB degradation with three times of cycling uses.

Besides Bi_2O_3 nanofibers, we have extended this method to prepare BiOCl nanofibers by electrospinning a precursor mixture of PAN/$BiCl_3$. Fig. 9 shows SEM image of as-spun PAN/$BiCl_3$ composite fibers (Fig. 9A) and BiOCl nanofibers (Fig. 9B). It can be seen that the diameters of PAN/$BiCl_3$ composite fibers range from 250 to 300 nm and the diameters of BiOCl nanofibers range from 80 to 140 nm, respectively. XRD pattern (Fig. S3) shows that the as-prepared BiOCl nanofibers calcined at 500 °C for 10 h can be well indexed to BiOCl (JCPDS file 85-861). FT-IR spectra (Fig. S4) suggests that PAN can be removed completely from PAN/$BiCl_3$ composite fibers after being calcined at 500 °C for 10 h, and a band corresponding to valent symmetrical, A_{2u}-type vibrations of Bi–O bond (515 cm^{-1}) in BiOCl [36] is observed, further indicating that the BiOCl nanofibers are obtained. XPS study (Fig. S5) reveals the presence of Bi, O and Cl in the BiOCl nanofibers. $Bi4f_{7/2}$ peak at 159.7 eV, $Bi4f_{5/2}$ peak at 164.9 eV, and Cl2p peak at 198.2 eV for BiOCl can be detected [37], indeed proving the formation of BiOCl nanofibers. UV–vis/DR analysis (Fig. S6) shows that the band gap energy for BiOCl is 3.2 eV. Meanwhile, the photoactivities of BiOCl nanofibers were tested and the results are shown in Fig. S7. It can be observed that RB can be degraded almost completely in the presence of BiOCl nanofibers for 60 min under UV light. The determined *k*r for BiOCl is 0.057 min^{-1}, indicating that BiOCl nanofibers exhibit good photocatalytic properties.

4. Summary

The Bi_2O_3 nanofibers with diameters of 70–200 nm were prepared by using the electrospun PAN/bismuth nitrate composite nanofibers as precursor through calcinations treatment. XRD, XPS, and UV–vis results suggest that β phase Bi_2O_3 were obtained after being calcined at 500 °C, and whereas a mixture of β phase Bi_2O_3 and α phase Bi_2O_3 as the minor phase were obtained after being calcined at 550–600 °C. Different temperatures result in different photocatalytic activites toward the photooxidation of RB. It has been found that Bi_2O_3 nanofibers calcined at 500 °C exhibit higher catalytic activity than that calcined at 550 and 600 °C, which can be attributed to their different phase composition, narrower band gap, smaller diameter and relatively high crystallinity. This study also provides a simple and inexpensive way to prepare other inorganic nanofibers photocatalysts such as BiOCl nanofibers on a large scale.

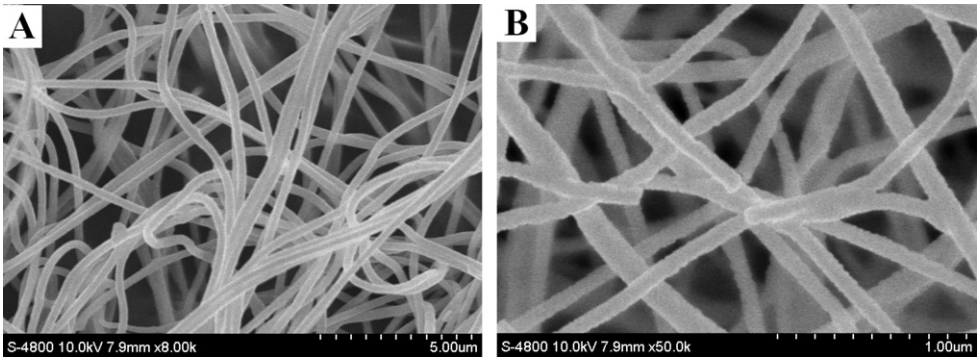

Fig. 9. SEM images of (A) as-spun PAN/$BiCl_3$ composite fibers, (B) BiOCl nanofibers.

Acknowledgments

This work is supported by National High Technology Research and Development Program of China (2006AA03Z311), Cultivation Found of the Key Scientific and Technical Innovation Project (Grant No. 704017), Ministry of Education of China, National Natural Science Foundation of China (Grant Nos. 60576040 and 50572014).

Supplementary material

The online version of this article contains additional supplementary material.

Please visit DOI: 10.1016/j.jcis.2008.12.077.

References

[1] J. Hu, M.Y. Ouyang, C.M. Lieber, Nature 399 (1999) 48.
[2] J.R. Heath, P.J. Kuekes, R.S. Williams, Science 280 (1998) 717.
[3] S.J. Chen, Y.C. Liu, C.L. Shao, R. Mu, Y.M. Lu, J.Y. Zhang, D.Z. Shen, X.W. Fan, Adv. Mater. 17 (2005) 586.
[4] M.R. Hoffmann, S.T. Martin, W. Choi, D.W. Bahnemann, Chem. Rev. 95 (1995) 69.
[5] D.S. Bhatkhande, V.G. Pangarkar, A.A.C.M. Beenackers, J. Chem. Technol. Biotechnol. 77 (2001) 102.
[6] O. Carp, C.L. Huisman, A. Reller, Prog. Solid State Chem. 32 (2004) 33.
[7] K. Maeda, T. Takata, M. Hara, N. Saito, Y. Inoue, H. Kobayashi, K. Domen, J. Am. Chem. Soc. 127 (2005) 8286.
[8] X. Chen, S.S. Mao, Chem. Rev. 107 (2007) 2891.
[9] X.H. Wu, W. Qin, W.D. He, J. Mol. Catal. A Chem. 261 (2006) 167.
[10] L.S. Zhang, W.Z. Wang, J. Yang, Z.G. Chen, W.Q. Zhang, L. Zhou, S.W. Liu, Appl. Catal. A Gen. 308 (2006) 105.
[11] Y. Bessekhouad, D. Robert, J.V. Weber, Catal. Today 101 (2005) 315.
[12] Z.Y. Liu, D.D. Sun, P. Guo, J.O. Leckie, Nano Lett. 7 (2007) 1081.
[13] S.H. Zhan, D.R. Chen, X.L. Jiao, C.H. Tao, J. Phys. Chem. B 110 (2006) 11199.
[14] D.V. Bavykin, J.M. Friedrich, F.C. Walsh, Adv. Mater. 18 (2006) 2807.
[15] H.Y. Guan, C.L. Shao, B. Chen, J. Gong, X.H. Yang, Inorg. Chem. Commun. 6 (2003) 1409.
[16] C.L. Shao, H.Y. Guan, Y.C. Liu, X.L. Li, X.H. Yang, J. Solid State Chem. 177 (2004) 2628.
[17] D. Li, Y.N. Xia, Adv. Mater. 16 (2004) 1151.
[18] X.F. Lu, Y.Y. Zhao, C. Wang, Adv. Mater. 17 (2005) 2485.
[19] O. Monnereau, L. Tortet, P. Llewellyn, F. Rouquerol, G. Vacquier, Solid State Ionics 157 (2003) 163.
[20] M. Gotić, S. Popović, S. Musić, Mater. Lett. 61 (2007) 709.
[21] H.W. Kim, J.W. Lee, S.H. Shim, Sens. Actuators B 126 (2007) 306.
[22] F. Miyaji, T. Yoko, S. Sakka, J. Non-Cryst. Solids 126 (1990) 170.
[23] R.J. Betsch, W.B. White, Spectrochim. Acta 34 (1978) 505.
[24] A. Bednarkiewicz, M. Maczka, W. Strek, J. Hanuza, M. Karbowiak, Chem. Phys. Lett. 418 (2006) 75.
[25] High Resolution XPS of Organic Polymers: The Scienta ESCA300 Database (1992).
[26] L.Q. Jing, H.G. Fu, B.Q. Wang, D.J. Wang, B.F. Xin, S.D. Li, J.Z. Sun, Appl. Catal. B 62 (2006) 282.
[27] P. Viswanathamurthi, N. Bhattarai, H.Y. Kim, D.R. Lee, Scripta Mater. 49 (2003) 577.
[28] S. Maensiri, W. Nuansing, Mater. Chem. Phys. 99 (2006) 104.
[29] M. Drache, P. Roussel, J.P. Wignacourt, Chem. Rev. 107 (2007) 80.
[30] L. Zhang, D.R. Chen, X.L. Jiao, J. Phys. Chem. B 110 (2006) 2668.
[31] X.H. Yang, C.L. Shao, H.Y. Guan, X.L. Li, J. Gong, Inorg. Chem. Commun. 7 (2004) 176.
[32] C.S. Turchi, D.F. Qllis, J. Catal. 122 (1990) 178.
[33] M.S. Lee, S.S. Park, G.D. Lee, C.S. Ju, S.S. Hong, Catal. Today 101 (2005) 283.
[34] C.H. Wang, A.F. Geng, Y.H. Guo, S.J. Jiang, X.S. Qu, L. Li, J. Colloid Interface Sci. 301 (2006) 236.
[35] D. Beydoun, R. Amal, G. Low, S. McEvoy, J. Nanopart. Res. 1 (1999) 439.
[36] M.N. Novokreshchenova, Yu. Yukhin, B.B. Bokhonov, Chem. Sustain. Devel. 13 (2005) 563.
[37] W.E. Morgan, W.J. Stec, J.R. Van Wazer, Inorg. Chem. 12 (1973) 953.